



# Controllable stepmotors and rectifiers of magnetic flux quanta

B.Y. Zhu<sup>a</sup>, F. Marchesoni<sup>a,b</sup>, V.V. Moshchalkov<sup>c</sup>, Franco Nori<sup>a,d,\*</sup>

<sup>a</sup> Frontier Research System, Digital Materials Lab., The Institute of Physical and Chemical Research (RIKEN),  
2-1 Hirosawa, Wako-shi, Saitama, 351-0198, Japan

<sup>b</sup> Istituto Nazionale di Fisica della Materia, Università di Camerino, I-62032 Camerino, Italy

<sup>c</sup> Laboratorium voor Vaste-Stoffysica en Magnetisme, K. U. Leuven, B-3001 Leuven, Belgium

<sup>d</sup> Center for Theoretical Physics, Physics Department, University of Michigan, Ann Arbor, MI 48109, USA

## Abstract

We study the transport of vortices in superconductors with square arrays of asymmetric pinning wells when applying an alternating electrical current. This system can induce a net rectifying or diode effect for the vortex motion, including collective stepmotor-type dynamics, where many vortices move forward a controlled and exact number of pin-lattice-spacings at each cycle of the AC driving force. This system exhibits a remarkable net DC response with striking sawtooth-type oscillations, which we have studied as a function of several parameters (e.g., field  $H$ , Amplitude of drive). We analytically derive the main numerical features obtained here.

© 2004 Elsevier B.V. All rights reserved.

**Keywords:** Superconducting vortex dynamics; Flux pinning; Vortex-motion control devices

## 1. Introduction

The control of the motion of vortices using asymmetric pinning [1–4] can be useful for applications in superconducting samples, including the removal of unwanted trapped flux in devices [5]. The control of flux motion can be used for flux pumps, rectifiers or diodes [1–4], as well as for the focusing and lensing of flux quanta in designated target regions within a superconducting device. Recently, several groups [1–4,6–12] have made proposals for quite distinct ways of using potential energy ratchets in superconductors. Most early

studies on ratchet-type systems focused on a *single* particle moving on a *1D* asymmetric potential, as opposed to *collective* motion in *2D* potentials (e.g., Refs. [1,3,4]).

Using analytical methods and molecular dynamics simulations, we study the stochastic rectification of AC-driven vortices due to the “ratchet effect” of asymmetric pinning sites. For instance, in contrast to the disordered case in Ref. [3], the regular structure studied here produces a DC Voltage from AC driven vortices for *any* value of  $H/H_1$ , not just for  $H/H_1 > 1$ . Here  $H_1$  is the field at which the total number of vortices  $N_v$  is equal to the number of strong (or weak) pinning sites  $N_p^s (= N_p^w)$ . More importantly, using two interpenetrating square pinning sublattices, it is possible to *easily and precisely control the collective motion of the vortices*. We obtain the crucial figure

\* Corresponding author. Tel.: +81484679707; fax: +8148-4679650.

E-mail address: [fnori@riken.jp](mailto:fnori@riken.jp) (F. Nori).

of merit  $\rho$  characterizing the performance of this type of devices. This asymmetry factor is proportional to the difference between the critical depinning forces,  $F_M - F_m$ . Here,  $F_m$  is the stopping force for vortex depinning when the driving force is directed from a strong pinning site to a weak one, and  $F_M$  in the opposite direction.

## 2. Model

The strong and the weak pinning sites are placed on two square sublattices with spacing  $a_0$  ( $= 1$  here) and separated a distance  $d$ . All pinning centers are modelled here by Gaussian potential wells (the model and notation are explained in detail in [13,14]) with a decay length  $R_p$ . The intensity of the individual pinning force is denoted by  $f_0 F_{p0}^{s,w}$  ( $s = \text{strong}$ ,  $w = \text{weak}$ ,  $F_{p0} = \text{pinning force strength}$ , measured in units of  $f_0$ ). The AC square-wave driving Lorentz force is  $\mathbf{F}_L = F_L^y(t)\hat{\mathbf{y}}$  and the repulsive vortex–vortex force is

$$\mathbf{F}_{vv}(\mathbf{r}_i) = F_{vv0} f_0 \sum_{j \neq i}^{N_v} \lambda \hat{\mathbf{r}}_{ij} / |\mathbf{r}_i - \mathbf{r}_j|, \quad (1)$$

where

$$\hat{\mathbf{r}}_{ij} = (\mathbf{r}_i - \mathbf{r}_j) / |\mathbf{r}_i - \mathbf{r}_j|.$$

The overdamped equation of motion [13–15] for vortex  $i$  is given by

$$\eta \mathbf{v}_i = \mathbf{F}_L + \mathbf{F}_{vv}(\mathbf{r}_i) + \mathbf{F}_p(\mathbf{r}_i). \quad (2)$$

The initial vortex positions are obtained from annealing. Parameters used in the simulations are  $R_p = 0.13a_0$ ,  $\lambda = 2.6a_0$ ,  $F_{vv0} = 0.1$ ,  $F_{p0}^s = 0.5$ ,  $d = 0.2a_0$  and  $F_{p0}^s F_{p0}^w = 2$ , time step  $\tau_0 = 1/150$ , and viscosity  $\eta = 1$ . Our results are insensitive to the sample size, typically  $10a_0 \times 10a_0$  (i.e.,  $N_p^w = N_p^s = 100$ ), provided that the density of vortices and pins remains unchanged.

## 3. Net DC voltage $V_{DC}$ versus AC drive period

Fig. 1(a) shows

$$V_{DC} = \sum_i^{N_v} v_i / N_v$$

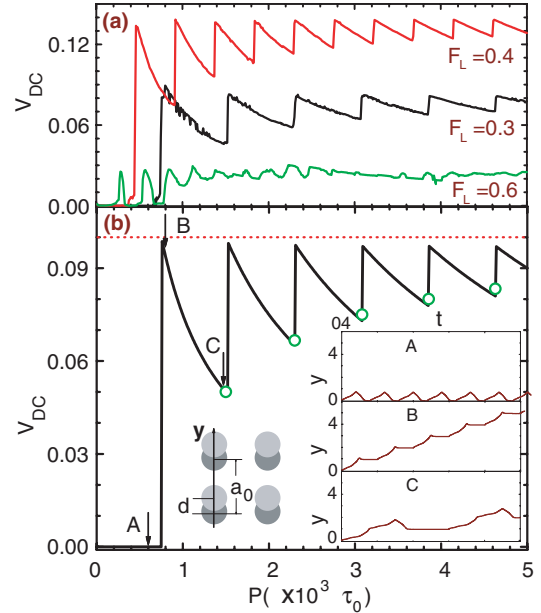


Fig. 1. (a) Net average DC velocity  $V_{DC}$  versus the half period  $P$  of the AC driving force for different amplitudes,  $F_L = 0.3, 0.4, 0.6$  for  $H/H_1 = 1.05$ . Notice the non-monotonic behavior of  $V_{DC}(P)$ , with the maximum  $V_{DC}$  obtained for  $F_L \sim 0.4$ . This unusual  $V_{DC}$  has a remarkable *sequence of jumps*. (b)  $V_{DC}$  versus  $P$  for  $F_L = 0.3$  for the first matching field,  $H/H_1 = 1$ . Analytically, we derive the horizontal dotted line  $V_M$ , and the open circles  $V_m(n)$ , for any  $n$ ; only  $n = 1$  through 5 are shown in (b). The inset shows the displacement  $y$  versus time ( $\times 10^3 \tau_0$ ) of any vortex for  $P/\tau_0 = 600$  (A), 800 (B) and 1500 (C) corresponding to the arrows in panel (b). A subset of the pinning array is also shown in (b).

for different amplitudes  $F_L$  of the driving force. Each plotted point is obtained by averaging over 200 periods, each with about  $10^4$ – $10^6$  time steps. Interestingly, when increasing the half period of the driving force (from  $P = 0$  to  $5000\tau_0$  with small step  $\Delta P = 10\tau_0$ ), sharp jumps in the rectified voltage  $V_{DC}(P)$  curves appear, mainly in the range  $F_m < F_L < F_M$ . When  $P$  is sufficiently small, the driven vortices travel a distance smaller than the minimum interpin distance  $a_0 - d - 2R_p$  during the first half-period  $P$  and, afterwards, the vortices will be driven back to the original pins during the second half-period, in the opposite direction of  $\mathbf{F}_L$ . This results in a trivial zero DC response of the vortices, as seen in Fig. 1(a). When the period of the driving force exceeds a threshold value  $P_c$ , which depends on  $F_L$ , the vortices move from one pinning site to a nearby

one during a half period and the system acts as a vortex rectifier. Moreover, it acts as a *controllable collective “stepmotor” of flux quanta*, where many vortices move forward in unison.

In the absence of both thermal noise and pinning force, a single vortex would alternate traveling a distance  $F_L \cdot P$  in one direction  $\mathbf{y}$  and then a distance  $F_L \cdot P$  in the other  $-\mathbf{y}$  direction. Thus, the minimum half-period  $P_c$  of the driving force  $F_L$  should be

$$P_c \sim a_0/F_L.$$

This is the reason why we obtain a threshold forcing period which clearly depends on  $F_L$ . The very unusual sawtooth-type oscillation of  $V_{DC}(P)$ , beyond the threshold  $P_c$  value, is a remarkable feature of this system. The very sharp peaks in  $V_{DC}$  indicate the location of the optimal forcing periods to achieve the maximum  $V_{DC}$ . The period  $P$  of the oscillation peaks in each curve is also dependent on  $F_L$ . Since the minimal spacing  $\tilde{P} \cdot F_L$  should also be  $\sim a_0$ , this means that the half period  $\tilde{P}$  of the  $V_{DC}(P)$  oscillation is almost the same as the critical threshold value  $P_c$  (see below for a more detailed discussion of why  $P_c \sim \tilde{P}$ ).

#### 4. Amplitude dependence of the net DC voltage

The net velocity  $V_{DC}$  depends non-monotonically (as in some other rectifiers [16]) on the amplitude  $F_L$  of the driving force (see Figs. 1(a) and 2). As seen in Fig. 2, For  $H/H_1 = 1.05$ , when  $F_L$  is larger than  $F_m \sim 0.23$ , the vortices can depin when

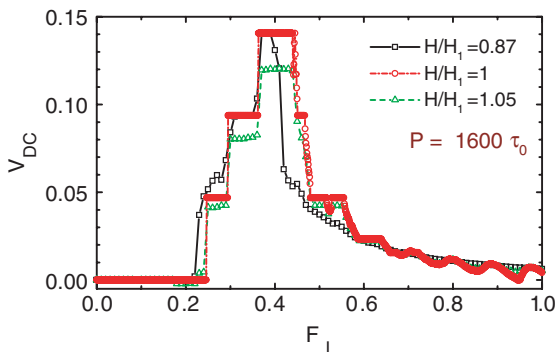


Fig. 2. Net velocity  $V_{DC}$  versus  $F_L$  for  $H/H_1 = 0.83$  (squares); 1 (circles); and 1.05 (triangles), with fixed half-period  $P = 1600\tau_0$ .

$F_L$  is parallel to the  $+y$ -axis. Of course, if the driving force is sufficiently large, all the vortices can move back and forth collectively regardless of the asymmetric pinning effect in the system, which results in the very weak DC response at  $F_L \simeq 0.6$  seen in Figs. 1(a) and 2. If the amplitude of the driving force is quite weak (i.e.,  $F_L < F_m$ ), the trapped vortices cannot be depinned in a period, which results in a highly suppressed DC response (i.e.,  $V_{DC} \sim 0$ ). In Fig. 1(b), we show  $V_{DC}$  for the first matching magnetic field,  $H/H_1 = 1$ , versus  $P$  for  $F_L = 0.3$ . The inset of Fig. 1(b) shows the displacement of any vortex versus time for the points A, B, and C indicated by the arrows in (b).

As seen in Fig. 2, with the increase of the amplitude  $F_L$  of the square-wave AC driving force, we find optimal  $F_L$  values for the DC response for  $H/H_1 = 0.83, 1.0$  and  $1.05$  with  $P = 1600\tau_0$ . Here, one can clearly note that when  $F_L$  is smaller than a critical value  $F_m$ , none of the trapped vortices can be depinned and no DC response can be measured. The amplitudes of the AC driving force that maximize the DC response are dependent on the ratio of the vortex density to the pins in the system. When  $H/H_1 = 1$ , the critical depinning force for the vortex motion is maximum and the rectifying or ratchet effect is most efficient for all the vortices, which reach their highest net DC velocities, as seen in Fig. 2. Each successive plateau corresponds to an additional pinning site explored by an increasing  $F_L$ . These turn into mild oscillations when the driving force  $F_L$  is strong enough.

For  $H/H_1 = 1$ ,  $V_{DC}(F_L)$  has very flat plateaus corresponding to commensurate lock-in transitions where the amplitude of the back-and-forth motion of the vortices matches the distance between pins. These lock-in plateaus are analogous to the “Arnold’s tongues” described in [15]. Away from the main lock-in plateaus,  $V_{DC}$  has a sharp drop. When  $H/H_1 > 1$ , due to the interstitial vortices which only cause a zero DC response, the pinning and the maximum  $V_{DC}$  are weaker.

#### 5. Comparison between AC and DC drives

It is instructive to compare the DC response between the AC drive and the difference between

two DC drives in two opposite directions along the  $y$ -axis. In Fig. 3(a), we show the stationary average vortex velocities  $V_R(F_L)$  and  $V_L(F_L)$ , as a function of the DC drive for  $\mathbf{F}_L \parallel \mathbf{y}$  and  $\mathbf{F}_L \parallel -\mathbf{y}$  at  $H/H_1 = 1.05$ , respectively ( $R = \text{Right}$  or  $+y$  and  $L = \text{left}$  or  $-y$ ). One can clearly see the asymmetric pinning effect for the vortex motion which depends on the orientation of the applied driving force in such composite strong and weak pinning arrays. Indeed, it is easier to depin vortices when driven in the positive direction ( $\mathbf{F} \parallel \mathbf{y}$ ) since the weaker pins are easier to overcome.

In Fig. 3(b), we show both the subtraction  $[V_R(F_L) - V_L(F_L)]/2$  from Fig. 3(a), which exhibits a sharp peak, and the net average DC response

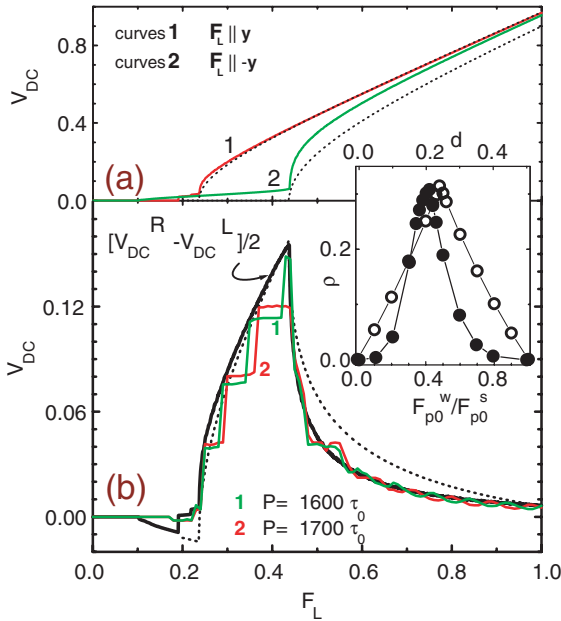


Fig. 3. Net average DC velocity  $V_{DC}$  versus  $F_L$  for: (a) DC current drive along  $y$  (curve 1) and  $-y$  (curve 2), and (b) AC drive along  $y$  (thin curves) for  $P/\tau_0 = 1600, 1700$ , and half the difference between the two DC-driven curves in (a) (thick curve). Here,  $H/H_1 = 1.05$ . Our one-particle predictions for  $u_{R,L}$  are plotted in (a) for comparison (dotted curves); the approximate adiabatic  $V_{DC}(F_L)$  is drawn in (b) as a dotted curve. The inset shows asymmetry factor  $\rho = (F_M - F_m)/(F_M + F_m)$  versus the ratio  $F_{p0}^w/F_{p0}^s$  (bottom axis) at  $F_{p0}^s = 0.5$  and  $d = 0.2a_0$  (open circles), and of the sublattice distance  $d$  (upper axis) for  $F_{p0}^s/F_{p0}^w = 2$  (solid circles). The asymmetry factor is proportional to the difference between the critical depinning forces. It is the *figure of merit* characterizing the performance of these devices.

$V_{DC}(F_L)$  for the AC driven case as a function of the amplitude  $F_L$  at fixed half periods  $P = 1600\tau_0$ , and  $1700\tau_0$ . Interestingly, the values of  $V_{DC}$  are always close to the value of  $[V_R - V_L]/2$ . This phenomenon has been revealed in some other ratchet systems [18,19].

## 6. Analytical analysis

A full analytical interpretation of the vortex ratchet flows simulated above lies beyond the reach of today's non-equilibrium statistical mechanics. Nevertheless, at  $H/H_1 = 1$  there are no interstitial vortices and therefore the overall vortex dynamics can be accurately analyzed through a simplified one-particle approach [16–19]. For  $H/H_1 = 1$  the effects of the vortex–vortex interaction cancel out for geometrical reasons, so we can just ignore them. The net potential  $U_p(y)$ , felt by a non-interacting vortex moving in the  $y$ -direction, results from the linear superposition of all pinning potentials along one lattice column. Thus,  $U_p(y)$  is a periodic asymmetric potential capable of sustaining a ratchet current [16–18]; in the absence of thermal fluctuations its rectifying power is mostly limited to the amplitude window  $[F_m, F_M]$ , with  $F_m < F_M$ . The two limiting values  $F_m$  and  $F_M$  (the maximum stopping forces along opposite directions) can be obtained from the expression of the pinning potential energy. We obtain  $F_m \approx 0.236$  ( $\sim 0.25 = F_{p0}^w$ ) and  $F_M \approx 0.436$  ( $\sim 0.5 = F_{p0}^s$ ) (see Fig. 3(a)). The inset in Fig. 3 shows the ratio of the difference between the stopping forces,  $F_M - F_m$ , over twice their average  $F_M + F_m$  as a function of both  $d$  and also  $F_{p0}^w/F_{p0}^s$ . This asymmetry factor is very clearly peaked at  $d \approx 0.21$  and  $F_{p0}^w/F_{p0}^s \approx 0.48$ .

The  $V_{DC}$  versus  $P$  curve for  $H/H_1 = 1$  in Fig. 1(b) can be reproduced fairly closely. First we need to determine the activation half-period  $P_c$ , when the rectification mechanism suddenly starts:  $P_c$  must be long enough for a single vortex to drift from one pinning well to the adjacent one along a  $y$ -column, by climbing the less steep side of the  $U_p(y)$  well it occupies. The net vortex velocity  $\langle u \rangle$  over such a distance is a nonlinear function of  $F_L$ . A rough estimate of  $\langle u \rangle$  can be given by assuming that the vortex velocity inside a pinning well tilted

in the positive direction, when  $F_L > F_m$ , is  $F_L - F_m$ , while in the flat region between pins is just  $F_L$  (recall that here  $\eta = 1$ ). The longitudinal size of the double pinning-well structure is about

$$\delta_p = 2R_p + d \quad (= 0.46a_0 \text{ here}),$$

hence

$$\langle u(F_L) \rangle = \kappa(F_L)F_L = F_L(1 - \delta_p F_m/F_L). \quad (3)$$

For the sake of comparison with our simulation data, the explicit value of the correcting factor is  $\kappa(F_L = 0.3) \simeq 0.64$ . Our estimate for the half period  $P_c$  becomes

$$P_c = a_0/\langle u \rangle = a_0/\kappa(F_L)F_L. \quad (4)$$

In Fig. 1(b),  $a_0 = 150\tau_0$ , therefore our analytical prediction for  $P_c$  yields  $P_c = 780\tau_0$ , within 2% of our simulation value.

The curve  $V_{DC}$  versus  $P$  in Fig. 1(b) shows a sequence of peaks of the same height  $V_{DC} = V_M$ . These peaks correspond to  $P = nP_c + \varepsilon$ , where  $\varepsilon$  is very small, i.e., to the driving condition when a single vortex can advance by  $n$  lattice constants  $a_0$  in the  $y$  direction during half a forcing cycle (getting immediately trapped as  $\mathbf{F}_L$  reverses its sign). The peak velocity is therefore

$$V_M = na_0/2nP_c = \kappa(F_L)F_L/2. \quad (5)$$

The minima  $V_m(n)$  of the curve  $V_{DC}$  versus  $P$  at  $H/H_1 = 1$  occur at

$$P = nP_c - \varepsilon,$$

as the vortex drifts a distance  $na_0$  in a half period of duration  $(n+1)P_c$ ; accordingly,

$$V_m(n) = V_M n/(n+1), \quad \text{with } n = 1, 2, 3, \dots \quad (6)$$

Both predictions for  $V_M$  and  $V_m(n)$  are displayed in Fig. 1(b) as compelling evidence for the one-particle approach when  $H/H_1 \sim 1$ .

In Fig. 2, for  $H/H_1 = 1$ , the first three horizontal steps of  $V_{DC}(F_L)$  have roughly similar widths  $\Delta F_L \sim 0.07$  and are equally spaced with  $\Delta V_{DC} \simeq 0.047$ . Both features are well reproduced by the heuristic argument in the equations for  $\langle u(F_L) \rangle$  and  $P_c$ . Periodic jumps in the  $V_{DC}(F_L)$  curve occur for

the discrete solutions  $F_L = F_n$  of the equation  $F\kappa(F)P_c = na_0$ , namely

$$F_n = nF_0 + \delta_p F_m, \quad (7)$$

with

$$F_0 = a_0/P = a_0/1600\tau_0 = 0.09375.$$

Only two jump amplitudes  $F_n$  fall *within* the rectification window  $[F_m, F_M]$ , i.e.  $F_2 = 0.30$  and  $F_3 = 0.36$  ( $F_1 \approx 0.2$  is shifted to 0.24, because  $V_{DC}$  is zero below  $F_m \sim 0.24$ ). As a consequence, the rising branch of  $V_{DC}(F_L)$  exhibits only three steps

$$V_{DC}(n) = n\Delta V_{DC},$$

with  $n = 1, 2, 3$  and  $\Delta V_{DC} \simeq 0.047$ . For  $P/\tau_0 = 3200$  (4800) we obtain six (nine) jumps within the rectification window (these plots will be shown elsewhere). The favorable comparison thus achieved establishes the validity of the Ansatz in our equation for  $\langle u(F_L) \rangle$  over the rectification window.

Finally, Fig. 3 also deserves closer inspection. The upper panel shows the stationary velocities  $V_{DC}^R = V_{DC}(+F_L)$  and  $V_{DC}^L = V_{DC}(-F_L)$  of a single vortex driven to opposite directions by a DC signal of intensity  $F_L$ . Ignoring the role of the unpinned vortices (here fewer than 5% since  $H/H_1 = 1.05$ ), we can try to extend the one-particle approach to this problem as well. The  $u(F_L)$  plot for a particle moving on a noiseless one-dimensional periodic substrate is reasonably well approximated by the formula

$$\begin{aligned} u_R(F_L) &= (F_L^2 - F_m^2)^{1/2} \quad \text{with } (F_L > F_m), \\ u_L(F_L) &= (F_L^2 - F_M^2)^{1/2} \quad \text{with } (F_L > F_M), \end{aligned} \quad (8)$$

which is exact in the case of a sinusoidal potential  $U_p(y)$  [18,19]. Here, one uses  $F_m$  if the vortex is being driven against the stopping force  $F_m$  (i.e., to the right) and vice versa. In Fig. 3(a) the agreement between  $V_{DC}^R$  and  $u_R$  is by far much closer than between  $V_{DC}^L$  and  $u_L$ . The reason for this discrepancy is twofold: (i) the pinning potential wells are too steep to be fitted by a sinusoidal function with appropriate amplitude and wavelength. Apparently, such an approximation works better for the lower slopes

encountered by a vortex being pulled in the opposite direction. (ii) Interstitial tails are easily detected in both curves  $V_{DC}^R$  and  $V_{DC}^L$ , with the interstitial effect looking more pronounced in the negative direction, i.e., for  $V_{DC}^L$  [13]. In Fig. 3(b) we compare the net velocity  $V_{DC}$  of the vortices subjected to a square wave periodic signal  $F_L(t)$  with the most obvious *adiabatic* approximation  $[V_{DC}^R - V_{DC}^L]/2$ . As shown in [18,19], the adiabatic curve (for  $P \rightarrow \infty$ ) embeds all the  $V_{DC}$  curves for finite  $P$ . Our formulae for  $u_{R,L}(F_L)$  can be used to reproduce the adiabatic curve from simulations, provided that one first adds an adequate interstitial tail to  $u_L(F_L)$ . For simplicity we fitted the interstitial tail of  $V_{DC}^L$  by means of a straight line  $u_L^i(F_L)$  for  $0 \leq F_L \leq F_M$  and a constant offset  $u_L^i(F_M) = 0.028$  for  $F > F_M$ ; the resulting adiabatic curve  $[u_R(F_L) - u_L(F_L) - u_L^i(F_L)]/2$  is plotted in Fig. 3(b) for the sake of a comparison.

Both adiabatic  $V_{DC}$  curves have a small *negative* current peak that, at low forcing amplitudes (from the simulation  $0.11 < F_L < 0.19$ ), drift in the  $-y$  direction. This reverse current is due to the interaction of the interstitial vortices with the pinned vortices. Note that the profile of the negative peak in the simulated adiabatic  $V_{DC}$  curve resembles the larger positive one. Indeed, we observed that in this forcing regime all interstitial vortices get trapped along pin lattice rows parallel to the  $y$  axis, thus forming soliton-like objects subject to an effective potential with lower stopping forces, but with a reversed asymmetry with respect to  $U_p(y)$ . When the bound vortices spend more time in the deeper wells, the asymmetry of the vortex-interaction-based “interstitial pinning” is *reversed*, since the interstitial vortices are “repelled” from the deeper (occupied) wells.

We have also studied [4,20] thermal effects (not shown here), but their only effect is to suppress the rectification at sufficiently large temperatures.

## 7. Summary

Finally, we emphasize that our results apply *mutatis mutandis* to arrays of Josephson junctions, colloidal systems, Wigner crystals and any system with repelling moveable objects that can be pinned by asymmetric traps.

## Acknowledgements

We acknowledge support from the Frontier Research System of RIKEN, Japan, and from the US National Science Foundation grant no. EIA-0130383. V.V.M. acknowledges the ESF Program “VORTEX”, the Belgian IUAP, Flemish GOA and FWO Programs. The visit of F.M. of the digital material laboratory (RIKEN) was supported by a Canon Foundation Award.

## References

- [1] J.F. Wambaugh et al., Phys. Rev. Lett. 83 (1999) 5106.
- [2] C.S. Lee et al., Nature 400 (1999) 337.
- [3] C.J. Olson et al., Phys. Rev. Lett. 87 (2001) 177002; W. Kwok et al., Physica C 382 (2002) 137.
- [4] B.Y. Zhu et al., Phys. Rev. B 65 (2003) 14514; F. Marchesoni et al., Physica A 325 (2003) 78; B.Y. Zhu et al., Physica C 388 (2003) 665; B.Y. Zhu et al., Physica E 18 (2003) 318; B.Y. Zhu et al., Physica E 18 (2003) 322.
- [5] H. Weinstock (Ed.), Applications of Superconductivity, Kluwer, Dordrecht, 1999; H. Weinstock (Ed.), SQUID Sensors, Kluwer, 1996.
- [6] I. Zapata et al., Phys. Rev. Lett. 77 (1996) 2292; I. Zapata et al., Phys. Rev. Lett. 80 (1998) 829.
- [7] S. Weiss et al., Europhys. Lett. 51 (2000) 499.
- [8] E. Goldobin et al., Phys. Rev. E 63 (2001) 031111.
- [9] E. Trías et al., Phys. Rev. E 61 (2000) 2257; H. Mooij et al., preprint.
- [10] F. Falo et al., Europhys. Lett. 45 (1999) 700.
- [11] G. Carapella et al., Phys. Rev. Lett. 87 (2001) 077002.
- [12] A flux-gradient-driven vortex diode using twin boundaries is described in J. Groth et al., Phys. Rev. Lett. 77 (1996) 3625.
- [13] B.Y. Zhu et al., Phys. Rev. B 64 (2001) 012504.
- [14] F. Nori, Science 271 (1996) 1373; C. Reichhardt et al., Phys. Rev. B 57 (1998) 7937.
- [15] C. Reichhardt et al., Phys. Rev. Lett. 82 (1999) 414.
- [16] P. Reimann, Phys. Rep. 361 (2002) 57; F. Julicher et al., Rev. Mod. Phys. 69 (1997) 1269; R.D. Astumian, Science 276 (1997) 917.
- [17] C.R. Doering et al., Phys. Rev. Lett. 72 (1994) 2984.
- [18] R. Bartussek et al., Europhys. Lett. 28 (1994) 459; F. Marchesoni, Phys. Rev. E 56 (1997) 2492; F. Marchesoni, Phys. Lett. A 237 (1998) 123.
- [19] M. Borromeo et al., Phys. Rev. E 65 (2002) 041110.
- [20] Color figures related to this work, and four illuminating color videos of the vortex motion, can be found at <http://www-personal.engin.umich.edu/~nori/stepmotor/>.